Fluid Mechanics
2016; 2(2): 13-27
http://www.sciencepublishinggroup.com/j/fm
doi: 10.11648/j.fm.20160202.11

Effect of Wall Conductivity on an Electric Conducting Fluid Flow Between Rotating and Stationary Coaxial Disks in the Presence of a Uniform Axial Magnetic Field

Toshio Tagawa

Department of Aerospace Engineering, Tokyo Metropolitan University, Tokyo, Japan

Email address:
tagawa-toshio@tmu.ac.jp (T. Tagawa)

To cite this article:
Toshio Tagawa. Effect of Wall Conductivity on an Electric Conducting Fluid Flow Between Rotating and Stationary Coaxial Disks in the Presence of a Uniform Axial Magnetic Field. *Fluid Mechanics.* Vol. 2, No. 2, 2016, pp. 13-27. doi: 10.11648/j.fm.20160202.11

Received: September 20, 2016; **Accepted**: October 14, 2016; **Published**: November 8, 2016

Abstract: Numerical analyses have been carried out for magnetohydrodynamic flow between a rotating and a stationary disk, whose radii are sufficiently large in comparison with the gap between the two parallel coaxial disks. The gap is filled with an electric conducting fluid and a uniform axial magnetic field is imposed. The magnetic Prandtl number is assumed to be so small that the influence of the induced magnetic field is neglected. The flow depends on both the rotational Reynolds number and the Hartmann number as well as the wall conductance ratios of upper and lower disks. As the Reynolds number increases, the core region of rigid body rotation having slight axial component of velocity is observed between the two boundary layers, whose thickness becomes thinner in proportional to the square root of the Reynolds number. On the other hand, as the Hartmann number increases, the Lorentz force tends to suppress the secondary flow significantly and boundary layer thickness of the azimuthal component of velocity is proportional to the inverse of the Hartmann number. The derived boundary condition for the normal component of electric current density at the interface allows us to obtain similarity solutions for various combinations of each wall conductance ratio and its influence on the flow is quite significant.

Keywords: Magnetohydrodynamics, Similarity Solution, Secondary Flow, Hartmann Number, Rotating Disk, Wall Conductance Ratio

1. Introduction

The research of the flow induced by an infinitely large rotating plain disk in the stationary fluid was commenced by von Kármán [1] who noticed that the radial and azimuthal components of the velocity are proportional to the radial distance from the center of axis and by which he revealed that the Navier-Stokes equations can be reduced to a set of ordinary differential equations (Kármán's transformation). Cochran [2] first successfully solved the set of ordinary differential equations numerically. On the contrary, Bödewadt *et al.* [3] investigated the boundary-layer flow, which is formed in the vicinity of the stationary plain disk fixed perpendicular to the rigid-body-rotation of fluid. These two boundary-layer rotating flows are known as typical non-linear self-similar solutions of the Navier-Stokes equation. However, the flow of Bödewadt's type is much more unstable than the single rotating disk flow of Kármán's type.

On the other hand, the flows between two coaxial rotating disks [4-13] exhibit more complicated phenomena than the two typical single-disk flows as mentioned above. The general treatment for this should consider that both disks are rotating at each angular velocity independently. However, for the sake of simplicity in terms of the reduction of input parameters, it is often the case that one disk is stationary and the opposing disk only rotates at a constant angular velocity. Apart from the single-disk flow, it is noted that the gap flow between the two disks varies its velocity profile depending on the Reynolds number based on the gap distance although it still keeps the Kármán's similarity. As increase in the Reynolds number, the flow tends to be divided into two boundary layers formed in the vicinity of the rotating and stationary disks respectively and a core region where the radial component of velocity is almost zero. The angular velocity of the core flow, which

accompanies slight axial flow from the Bödewadt layer (stationary disk) to the Kármán layer (rotating disk), is about 30% of that of the rotating disk.

Concerning the effect of the applied magnetic field on such disk flows, Davidson and Pothérat [14] investigated details of Bödewadt-Hartmann flow for a single-disk case. Moresco and Alboussière [15] performed a linear stability analysis of the MHD Bödewadt flow. Stephenson [16] studied liquid metal flow between the rotating and stationary coaxial disks in the presence of a uniform axial magnetic field with the analysis of similar solution as well as the experiment using mercury. Kamiyama and Sato [17] investigated a similar system to Stephenson's study with considering the effect of wall-conductance of disks. They limited their theoretical analyses to the case that the interaction parameter is much larger than unity ($N >> 1$), which enables to derive approximate solutions by expanding each variable such as velocity and pressure in powers of $1/N$. Magnetohydrodynamic flow between a rotating disk and a stationary disk with the effect of suction from the porous disk were numerically investigated in the references [18, 19]. However, no studies have been considered for the effect of wall conductivity with large Reynolds number cases. In this paper, the characteristic of the fluid flow at relatively high Reynolds numbers between the two coaxial disks in the presence of a uniform axial magnetic field is numerically studied together with the consideration of wall-conductance of disks.

2. Governing Equations

Figure 1 shows the schematic model for the present problem considered. The upper disk whose thickness is t_K, is rotating at a constant angular velocity while the lower disk whose thickness is t_B, is stationary. We assume that the working fluid between the two coaxial disks is an incompressible, Newtonian, electric conducting fluid, and it is subjected to a uniform axial magnetic field. The effect of the viscous dissipation, the Joule heat and the induced magnetic field on the flow is neglected. The gap distance between the two disks is d, which is sufficiently small in comparison with the radius of the disks. Therefore, we expect that the Kármán's similarity is valid even in the present problem except near the edge of disks, i.e. the flow and electromagnetic fields are axisymmetric and their radial and azimuthal components are proportional to the radial location from the center of rotating axis. The assumption of the Kármán's similarity in this problem allows us to derive a set of ordinary differential equations, whose solution can be numerically computed with high accuracy owing to the reduction of the dimension. The most crucial point in this problem is to obtain both the radial pressure gradient and electric potential gradient. As will be mentioned later, the radial pressure gradient and the radial electric field are not functions of axial location but constants due to the assumption of the Kármán's similarity.

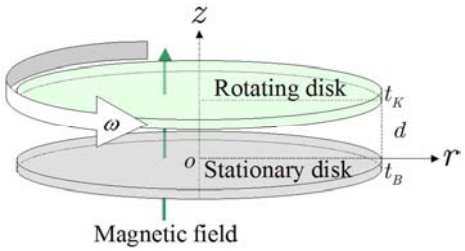

Figure 1. *Schematic of the problem considered. The upper disk whose thickness is t_K is rotating at a constant angular velocity ω, while the lower disk whose thickness is t_B is stationary. The gap space between the two disks is filled with an electric conducting fluid and an external uniform axial magnetic field is imposed.*

The followings show the axisymmetric Navier-Stokes equation in the cylindrical coordinate system.

$$\frac{\partial u}{\partial r}+\frac{u}{r}+\frac{\partial w}{\partial z}=0 \tag{1}$$

$$\begin{aligned} &u\frac{\partial u}{\partial r}+w\frac{\partial u}{\partial z}-\frac{v^2}{r} \\ &=-\frac{1}{\rho}\frac{\partial p}{\partial r}+\nu\left(\frac{\partial^2 u}{\partial r^2}+\frac{1}{r}\frac{\partial u}{\partial r}-\frac{u}{r^2}+\frac{\partial^2 u}{\partial z^2}\right)+\frac{f_R}{\rho} \end{aligned} \tag{2}$$

$$u\frac{\partial v}{\partial r}+w\frac{\partial v}{\partial z}+\frac{uv}{r}=\nu\left(\frac{\partial^2 v}{\partial r^2}+\frac{1}{r}\frac{\partial v}{\partial r}-\frac{v}{r^2}+\frac{\partial^2 v}{\partial z^2}\right)+\frac{f_\theta}{\rho} \tag{3}$$

$$u\frac{\partial w}{\partial r}+w\frac{\partial w}{\partial z}=-\frac{1}{\rho}\frac{\partial p}{\partial z}+\nu\left(\frac{\partial^2 w}{\partial r^2}+\frac{1}{r}\frac{\partial w}{\partial r}+\frac{\partial^2 w}{\partial z^2}\right)+\frac{f_Z}{\rho} \tag{4}$$

Each component of the external force appeared in the momentum equations indicates the electromagnetic force. To obtain the electromagnetic force, each component of electric current density governed by the conservation of electric charge and the Ohm's law is given as follows:

$$\frac{\partial j_R}{\partial r}+\frac{j_R}{r}+\frac{\partial j_Z}{\partial z}=0 \tag{5}$$

$$j_R=\sigma\left(-\frac{\partial \psi}{\partial r}+vb_0\right) \tag{6}$$

$$j_\theta=-\sigma u b_0 \tag{7}$$

$$j_Z=-\sigma\frac{\partial \psi}{\partial z} \tag{8}$$

The electromagnetic force incorporated in the momentum equations is given as follows:

$$\begin{aligned} \vec{f}&=\vec{j}\times\vec{B}=\left(j_R\vec{e}_R+j_\theta\vec{e}_\theta+j_Z\vec{e}_Z\right)\times b_0\vec{e}_Z \\ &=\left(f_R\right)\vec{e}_R+\left(f_\theta\right)\vec{e}_\theta+\left(f_Z\right)\vec{e}_Z \\ &=\left(j_\theta b_0\right)\vec{e}_R+\left(-j_R b_0\right)\vec{e}_\theta+\left(0\right)\vec{e}_Z \\ &=-\sigma u {b_0}^2\vec{e}_R-\sigma b_0\left(-\frac{\partial \psi}{\partial r}+vb_0\right)\vec{e}_\theta \end{aligned} \tag{9}$$

The boundary condition for the electric current density at the rotating disk is illustrated in Fig. 2. The upper side of the disk is insulating while the lower side is facing to an electro-conducting fluid. It is assumed that the tangential

electric current density is constant over the thickness of the disk.

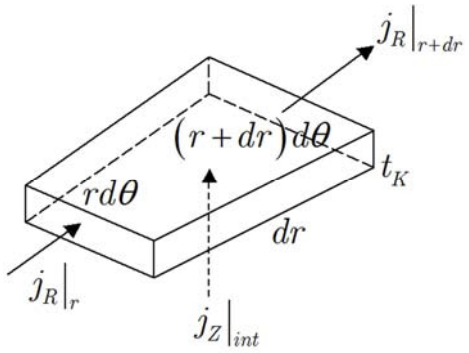

Figure 2. *The electric current density balance within an infinitesimal element for the conducting wall at the rotating disk.*

The electric current density balance within an infinitesimal element for the conducting disk is as follows.

$$rd\theta \cdot t_K \cdot j_R\big|_r + rd\theta \cdot dr \cdot j_Z\big|_{int} = (r+dr)\,d\theta \cdot t_K \cdot j_R\big|_{r+dr} \tag{10}$$

Using of the Taylor expansion,

$$j_R\big|_{r+dr} \cong j_R\big|_r + \left.\frac{\partial j_R}{\partial r}\right|_r dr \tag{11}$$

Taking Eqs. (10) and (11) into account, the normal component of electric current density at the interface is written as

$$j_Z\big|_{int} \cong \frac{t_K}{r}\left(r\left.\frac{\partial j_R}{\partial r}\right|_r + j_R\big|_r\right) = \frac{t_K}{r}\frac{\partial}{\partial r}\left(r\, j_R\big|_r\right). \tag{12}$$

The radial electric current density within the rotating disk is given by the Ohm's law.

$$j_R\big|_r = \sigma_K\left(-\frac{\partial \psi}{\partial r} + \omega b_0 r\right) \tag{13}$$

Combining Eqs. (12) and (13) and assuming the uniformity of electric conductivity of the disk, we can obtain the normal component of electric current density as follows:

$$\begin{aligned} j_Z\big|_{int} &\cong \frac{t_K}{r}\frac{\partial}{\partial r}\left(r\, j_R\big|_r\right) = -\frac{\sigma_K t_K}{r}\frac{\partial}{\partial r}\left(r\frac{\partial \psi}{\partial r} - \omega b_0 r^2\right) \\ &= -\sigma_K t_K\left(\frac{\partial^2 \psi}{\partial r^2} + \frac{1}{r}\frac{\partial \psi}{\partial r} - 2\omega b_0\right) \end{aligned} \tag{14}$$

Finally, the boundary conditions at the rotating disk and stationary disk are summarized as follows together with three velocity components.

$$\begin{cases} z = d: \quad u = 0,\ v = \omega r,\ w = 0, \\ \quad j_Z = -\sigma_K t_K\left(\dfrac{\partial^2 \psi}{\partial r^2} + \dfrac{1}{r}\dfrac{\partial \psi}{\partial r} - 2\omega b_0\right) \\ z = 0: \quad u = 0,\ v = 0,\ w = 0, \\ \quad j_Z = \sigma_B t_B\left(\dfrac{\partial^2 \psi}{\partial r^2} + \dfrac{1}{r}\dfrac{\partial \psi}{\partial r}\right) \end{cases} \tag{15}$$

3. Dimensionless Equations

By considering the following Karman's similarity for the three components of velocity

$$Z = \frac{z}{d},\ U(Z) = \frac{u(r,z)}{\omega r},\ V(Z) = \frac{v(r,z)}{\omega r},\ W(Z) = \frac{w(z)}{\omega d} \tag{16}$$

and by differentiating with respect to *r* for Eq. (4), it yields that the radial pressure gradient is not a function of *z*.

$$\frac{\partial}{\partial z}\left(\frac{\partial p(r,z)}{\partial r}\right) = 0 \tag{17}$$

The radial component of the momentum equation in a dimensionless form can be expressed as

$$\begin{aligned} &U^2 - V^2 + W\frac{dU}{dZ} - \frac{1}{Re}\frac{d^2U}{dZ^2} + \frac{Ha^2}{Re}U \\ &= -\frac{1}{\rho r\omega^2}\underbrace{\frac{\partial p(r,z)}{\partial r}}_{f(r)} = \text{const.} \end{aligned} \tag{18}$$

The left-hand-side is a function of *z*, while the right-hand-side is a function of *r*. Therefore, both should be a constant to satisfy the double requirements. As indicated in Eq. (19), the dimensionless radial pressure gradient must be a constant.

$$P_R \equiv \frac{1}{\rho r\omega^2}\frac{\partial p(r,z)}{\partial r} = \frac{f(r)}{\rho\omega^2 r} = \frac{k_p}{\rho\omega^2} = \text{const.} \tag{19}$$

Therefore, the pressure can be expressed as summation of a function of *r* and a function of *z* as follows.

$$p(r,z) = \underbrace{\frac{1}{2}k_p r^2}_{p_1(r)} + p_2(z) \tag{20}$$

Considering Eq. (20), the axial component of momentum equation can be rewritten as follows:

$$w\frac{dw}{dz} = -\frac{1}{\rho}\frac{dp_2}{dz} + \nu\frac{d^2w}{dz^2} \tag{21}$$

This equation can be expressed in a dimensionless form as follows:

$$W\frac{dW}{dZ} = -\frac{dP}{dZ} + \frac{1}{Re}\frac{d^2W}{dZ^2} \tag{22}$$

where, the dimensionless pressure is defined as follows.

$$P(Z) = \frac{p_2(z)}{\rho\omega^2 d^2} \tag{23}$$

Eq. (20) is rewritten as follows:

$$\begin{aligned} p(r,z) &= p_1(r) + p_2(z) \\ &= \frac{1}{2}k_p r^2 + \rho\omega^2 d^2 \cdot P(Z) \end{aligned} \tag{24}$$

Next, by applying the Karman's similarity to the components of electric current density

$$J_R(Z)=\frac{j_R(r,z)}{\sigma\omega b_0 r},\ J_\theta(Z)=\frac{j_\theta(r,z)}{\sigma\omega b_0 r},\ J_Z(Z)=\frac{j_Z(z)}{\sigma\omega b_0 d} \tag{25}$$

and by differentiating with respect to r for Eq. (8), it is recognized that the radial potential gradient is not a function of z.

$$\frac{\partial}{\partial z}\left(\frac{\partial\psi(r,z)}{\partial r}\right)=0 \tag{26}$$

The radial component of the Ohm's law in a dimensionless form can be expressed as follows.

$$J_R-V=-\frac{1}{\omega b_0 r}\underbrace{\frac{\partial\psi(r,z)}{\partial r}}_{g(r)} \tag{27}$$

The left-hand-side is a function of z, while the right-hand-side is a function of r. As shown in Eq. (28), the dimensionless radial potential gradient must be a constant.

$$\Psi_R\equiv\frac{1}{\omega b_0 r}\frac{\partial\psi(r,z)}{\partial r}=\frac{g(r)}{\omega b_0 r}=\frac{k_\psi}{\omega b_0}=\text{const.} \tag{28}$$

Therefore, the electric potential can be expressed as summation of a function of r and a function of z as follows.

$$\psi(r,z)=\underbrace{\frac{1}{2}k_\psi r^2}_{\psi_1(r)}+\psi_2(z) \tag{29}$$

Therefore, Eq. (8) can be rewritten as follows:

$$j_Z=-\sigma\frac{d\psi_2}{dz} \tag{30}$$

This equation can be written in a dimensionless form as follows:

$$J_Z=-\frac{d\Psi}{dZ} \tag{31}$$

where, the dimensionless electric potential is as follows.

$$\Psi(Z)=\frac{\psi_2(z)}{\omega b_0 d^2} \tag{32}$$

Eq. (29) is written

$$\psi(r,z)=\psi_1(r)+\psi_2(z)=\frac{1}{2}k_\psi r^2+\omega b_0 d^2\cdot\Psi(Z) \tag{33}$$

A set of dimensionless ordinary differential equations and the boundary conditions are summarized as follows:

$$2U+\frac{dW}{dZ}=0 \tag{34}$$

$$U^2-V^2+W\frac{dU}{dZ}=-P_R+\frac{1}{Re}\frac{d^2U}{dZ^2}-\frac{Ha^2}{Re}U \tag{35}$$

$$2UV+W\frac{dV}{dZ}=\frac{1}{Re}\frac{d^2V}{dZ^2}-\frac{Ha^2}{Re}\left(-\Psi_R+V\right) \tag{36}$$

$$W\frac{dW}{dZ}=-\frac{dP}{dZ}+\frac{1}{Re}\frac{d^2W}{dZ^2} \tag{37}$$

$$2J_R+\frac{dJ_Z}{dZ}=0 \tag{38}$$

$$J_R=-\Psi_R+V \tag{39}$$

$$J_\theta=-U \tag{40}$$

$$J_Z=-\frac{d\Psi}{dZ} \tag{41}$$

The boundary conditions at the interfaces between the fluid layer and the disks, and the outside of the two disks are given respectively as follows:

$$\begin{cases} Z=1:\ U=0,\ V=1,\ W=0, \\ \quad J_Z=-2C_K\left(\Psi_R-1\right) \\ Z=0:\ U=0,\ V=0,\ W=0, \\ \quad J_Z=2C_B\Psi_R \end{cases} \tag{42}$$

$$\begin{cases} Z=1+t_K/d:\ J_Z=0 \\ Z=-t_B/d:\ J_Z=0 \end{cases} \tag{43}$$

Finally the dimensionless variables are modified as follows:

$$\begin{aligned} &Z=\frac{z}{d},\ U(Z)=\frac{u(r,z)}{\omega r},\ V(Z)=\frac{v(r,z)}{\omega r}, \\ &W(Z)=\frac{w(z)}{\omega d},\ P(Z)=\frac{p(r,z)-k_p r^2/2}{\rho\omega^2 d^2}, \\ &P_R=\frac{k_p}{\rho\omega^2},\ J_R(Z)=\frac{j_R(r,z)}{\sigma\omega b_0 r},\ J_\theta(Z)=\frac{j_\theta(r,z)}{\sigma\omega b_0 r}, \\ &J_Z(Z)=\frac{j_Z(z)}{\sigma\omega b_0 d},\ \Psi(Z)=\frac{\psi(r,z)-k_\psi r^2/2}{\omega b_0 d^2},\ \Psi_R=\frac{k_\psi}{\omega b_0} \end{aligned} \tag{44}$$

The non-dimensional numbers are the Hartmann number, the Reynolds number based on the angular velocity of the rotating disk, and conductance ratios for the rotating disk and the stationary disk.

$$Ha=b_0 d\sqrt{\frac{\sigma}{\rho\nu}},\ Re=\frac{\omega d^2}{\nu},\ C_K=\frac{\sigma_K t_K}{\sigma d},\ C_B=\frac{\sigma_B t_B}{\sigma d} \tag{45}$$

4. Computational Strategy

Under the boundary conditions of Eq. (42), the simultaneous ordinary differential equations are discretized and numerically solved on a one-dimensional grid system using the central difference method for all the terms in Eqs. (34) - (41). From Eqs. (35) and (36), the radial and azimuthal components of velocity was obtained iteratively using the Jacobi method during which Eq. (34) was used to obtain the axial velocity. Although the pressure does not influence on the system of the simultaneous differential equations, if necessary it can be obtained from Eq. (37) by integrating with respect to Z. Eqs. (38) – (41) are necessary for getting the three components of electric current density and electric potential but they are independent of the electromagnetic force terms in the momentum equations. As easily recognized from Eq. (34) and the boundary condition of the axial velocity, the integration over the fluid layer for the radial velocity must be zero.

$$\int_0^1 U\,dZ = 0 \tag{46}$$

Therefore, the pressure gradient P_R appeared in Eq. (35) can be obtained by the use of Eq. (46) as follows.

$$P_R = \int_0^1 \left(-U^2 + V^2 - W\frac{dU}{dZ} + \frac{1}{Re}\frac{d^2U}{dZ^2} \right) dZ \tag{47}$$

On the other hand, the potential gradient Ψ_R appeared in Eq. (39) should be obtained to satisfy the integrated value of the radial electric current over the two disks and the fluid layer would be zero.

$$\int_{-t_B/d}^{0} \frac{\sigma_B}{\sigma}(-\Psi_R)\,dZ + \int_0^1 (-\Psi_R + V)\,dZ + \int_1^{1+t_K/d} \frac{\sigma_K}{\sigma}(-\Psi_R + 1)\,dZ = 0 \tag{48}$$

As a consequence, the potential gradient Ψ_R is shown in Eq. (49).

$$\Psi_R = \left(\int_0^1 V\,dZ + C_K \right) \Big/ (C_B + 1 + C_K) \tag{49}$$

From this equation, we recognize that the radial potential gradient is influenced by the wall conductance ratios of both rotating and stationary disks. Specific computational examples for several combinations of the wall conductance are illustrated in section 5.4. The number of grids in the Z-direction is 512 and the obtained results are almost identical to the cases having more number of grids.

5. Numerical Results

5.1. Validity of the Present Computational Method

Figure 3 shows comparison between the previous study done by Stephenson [16] and the present results for the Reynolds number 176 with several cases of Hartmann number to ensure the validity of the present code utilized in this study. In order to meet the Stephenson's configuration, the upper boundary indicates the stationary disk and the lower boundary is the rotating disk. Both disks are electrically insulated. For all the cases, the present results agree with the Stephenson's results.

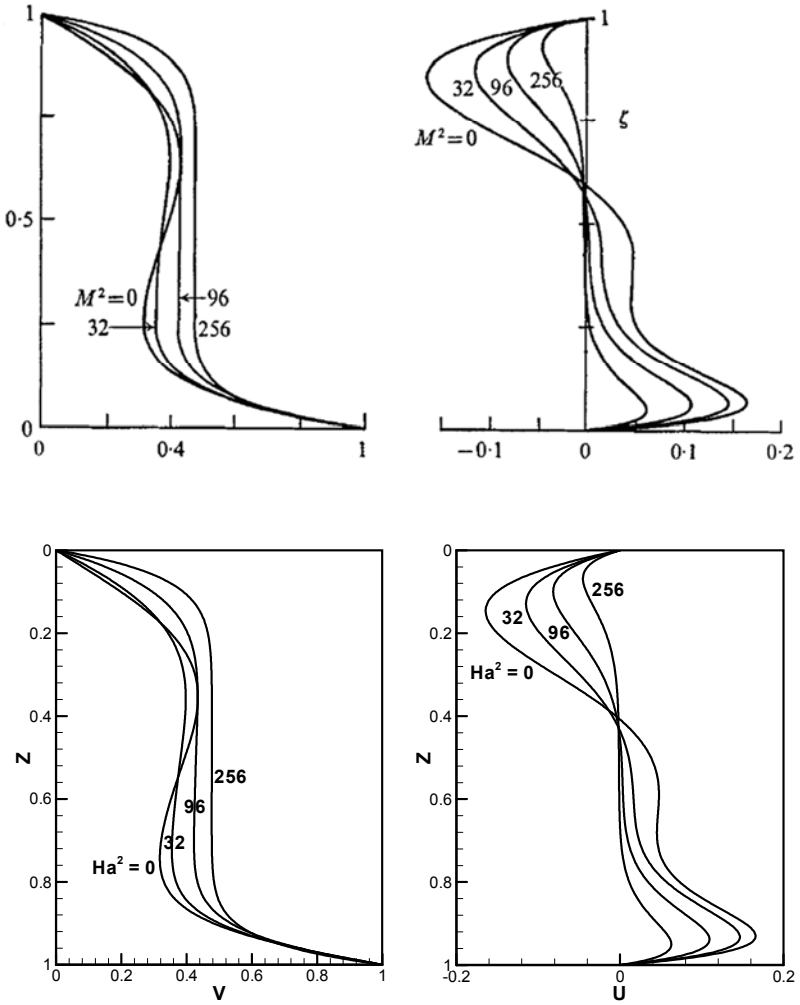

Figure 3. *Comparison of the azimuthal and radial components of velocity profiles between the Stephenson's (upper) and present (lower) results for Re = 176. Note that a lower disk is rotated and an opposing upper disk is held at rest. M indicates the Hartmann number.*

5.2. Without Magnetic Field

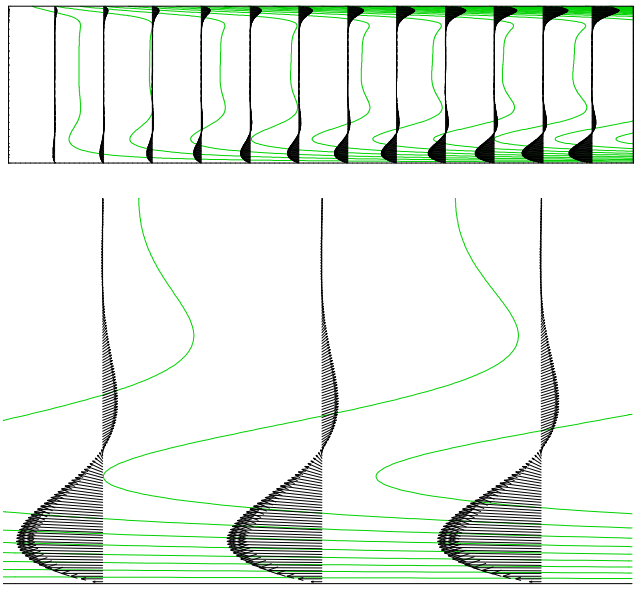

Figure 4. *A two-dimensional visualization of the velocity field at Re = 1000 and Ha = 10. The black arrows represent the secondary velocity and the green contour lines indicate the azimuthal velocity. The left end is the center axis of rotation.*

Figure 4 shows an example of two-dimensional visualization for understanding the whole feature of the flow at $Re = 1000$ and $Ha = 0$. The arrows indicate the meridional flow and the contour lines indicate the azimuthal flow. It is recognized that the radial and azimuthal velocity components are proportional to the distance from the center axis of rotation while the axial component of velocity is constant and independent of radial location. In the vicinity of the upper rotating disk the radially-outward flow takes place while in the lower boundary layer the radially-inward flow appears. Since this analysis supposes the similarity flow, it cannot predict the stability of the flow. In general, the lower boundary layer is less stable than the upper boundary layer and it exhibits flow transition from laminar to turbulent as increase in the radial distance from the center axis of rotation. We will not mention the stability of the flow but will show some basic flows in the subsequent sections.

Figure 5 shows (a) radial, (b) azimuthal, (c) axial components of velocity, and (d) pressure distribution for various values of the Reynolds number as indicated in the figures. In the limit of the small Reynolds number, the radial and axial components of velocity are zero and azimuthal velocity exhibits the linear profile. When the Reynolds number exceeds 1000 or so, the distinct boundary layers and a core region are formed. In such high Reynolds number cases, the thickness of the layers is proportional to the inverse of the square root of the Reynolds number. Within the Kármán layer formed in the vicinity of the rotating disk at $Z = 1$, radially-outward flow is induced due to the centrifugal force. On the contrary, within the Bödewadt layer formed in the vicinity of the stationary disk at $Z = 0$, an oscillatory velocity distribution in the radial and azimuthal components is observed.

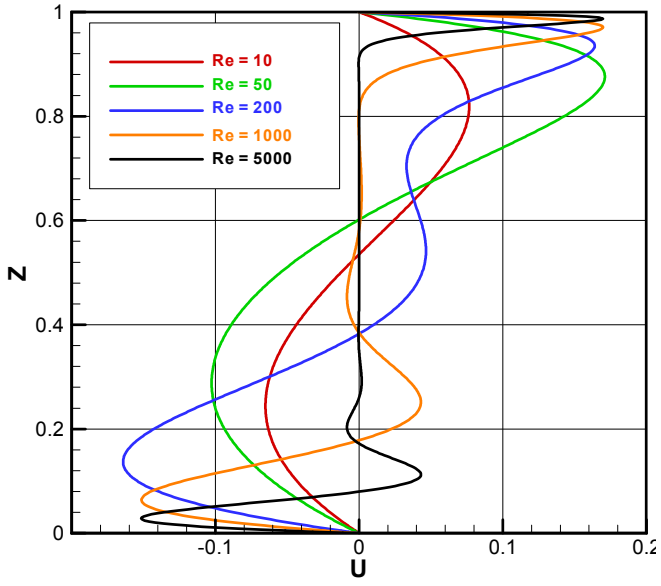

(a)

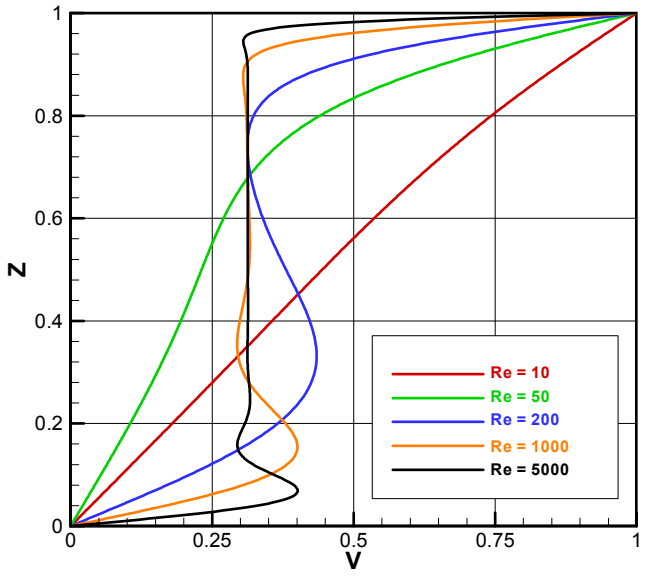

(b)

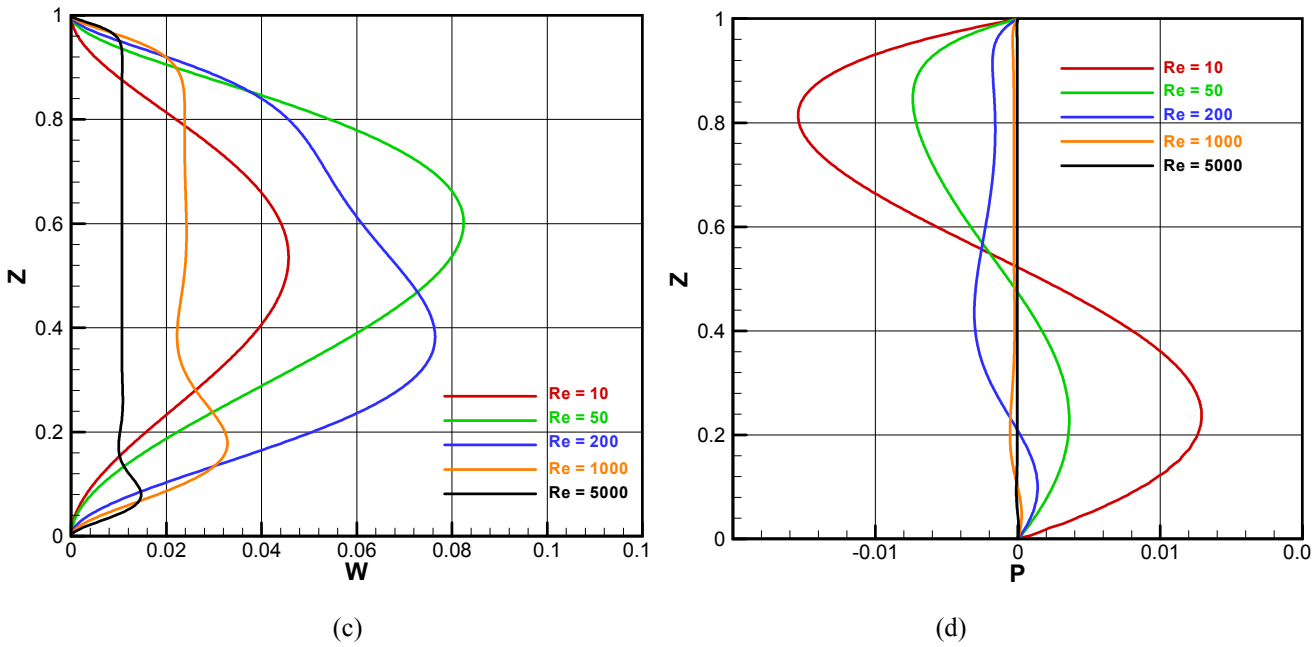

(c) (d)

Figure 5. *The velocity and pressure profiles for the various Reynolds numbers at Ha = 0. (a) Radial component of velocity, (b) Azimuthal component of velocity, (c) Axial component of velocity, (d) Pressure.*

The characteristic of the boundary layers in the present coaxial two-disk flow qualitatively agrees with that of single disk flow such as the Kármán flow or the Bödewadt flow. According to the present numerical results, in the limit of the high Reynolds number cases, the azimuthal component of velocity at the core region indicates $V_c = 0.313$ and the axial one $W_c = 0.755 / Re^{0.5}$. The value of pressure in the core region can be directly obtained from the axial velocity as $P_c = - 0.285 / Re$. Let us compare the numerical results of the present two-disk flow in the limit of the high Reynolds number case with those of single-disk flows. According to the present result using a code of single-disk flows, the Kármán flow indicates that $W_c = 0.8845 / Re^{0.5}$, $P_c = - 0.3911 / Re$, while the Bödewadt flow indicates $W_c = 1.350 / Re^{0.5}$, $P_c = - 0.9107 / Re$. This suggests that those values in the single-disk flows are greater than those in the present two-disk flow. Table 1 summarizes such values of velocity in the core region together with the values of azimuthal velocity gradient at each wall.

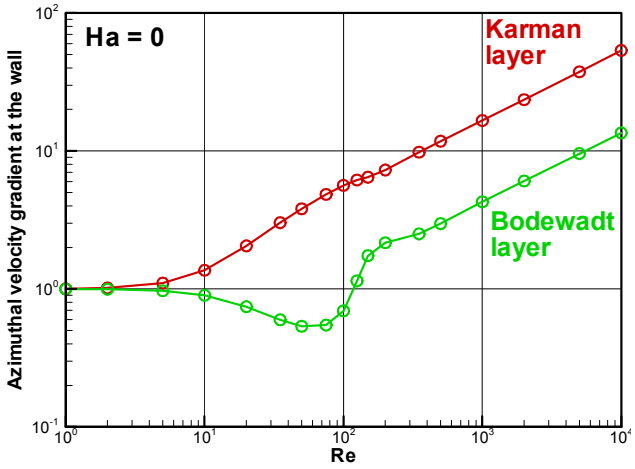

Figure 6. *The azimuthal velocity gradient at the walls for the various Reynolds numbers at Ha = 0.*

Table 1. *Asymptotic values obtained for the large Reynolds number limit in the absence of magnetic field.*

	Single-disk flow		Present two-disk flow	
	Kármán flow	**Bödewadt flow**	**Kármán layer**	**Bödewadt layer**
U_w'	$0.5102\ Re^{0.5}$	$0.9420\ Re^{0.5}$	$0.510\ Re^{0.5}$	$0.170\ Re^{0.5}$
V_w'	$0.6159\ Re^{0.5}$	$0.7728\ Re^{0.5}$	$0.526\ Re^{0.5}$	$0.135\ Re^{0.5}$
V_c	0.000	1.000	0.313	
W_c	$0.8845 / Re^{0.5}$	$1.350 / Re^{0.5}$	$0.755 / Re^{0.5}$	
P_c	$0.3911 / Re$	$0.9107 / Re$	$0.285 / Re$	

Appendix A shows the detailed description of the governing equations and the numerical results of the tangential velocities for several values of N.

Figure 6 shows the azimuthal velocity gradient at each boundary as a function of the Reynolds number. The velocity gradient at the Kármán layer is larger than that at the Bödewadt layer. For the Reynolds number more than 1000 or so, it is recognized that the azimuthal velocity gradient at each layer is proportional to the square root of the Reynolds number. For the moderate Reynolds number, the two layers interact with each other, and thus the Bödewadt layer exhibits a complicated behavior.

5.3. Influence of the Axial Uniform Magnetic Field

Figure 7 shows the velocity, electric current and potential profiles at N = 0.3. Although the value of the interaction parameter is not very large, it is recognized that there is substantial influence on the velocity profile. In (a), the radial velocity tends to be damped. As will be mentioned, the core velocity seems to be zero at a glance but it deviates slightly from zero depending on the values of the non-dimensional parameters. Hence, the core flow at the high Reynolds number is slightly different from the flow of rigid-body-rotation which was observed in the non-magnetic cases. In (b), the core velocity tends to be a constant value for the cases of the larger Reynolds number. In (c), the axial velocity is not directly influenced by the Lorentz force but is damped to some extent due to the reduction of the radial velocity affected by the Lorentz force. As a consequence, the secondary flow tends to be damped. It is noted that the axial core velocity profile at the high Reynolds number cases exhibits slight inclination. This implies that radial core velocity is not exactly zero because of the mass conservation given in Eq. (34). In (d), the radial component of electric current density J_R is equivalent to the one shifted in the amount of radial electric field from the azimuthal velocity as suggested in Eq. (39). The amount of radial electric field depends on the Reynolds and Hartmann numbers. The radial component of electric current density is included in Eq. (36) as an external force term, and although the absolute value is not very large, this Lorentz force must keep a state of balance with other terms. Therefore, the radial velocity cannot keep zero and the balance between the Lorentz force and inertial force takes place. In (e), the axial electric current density in the core region for the large Reynolds number cases is not a constant but is inclined. This implies that there is the azimuthal Lorentz force balancing with the azimuthal inertial force ($2UV$) as can be recognized from Eqs. (36) and (38). In (f), the electric potential indicates the value of integration of J_Z. The axial electric current flows from the stationary disk to the rotating disk.

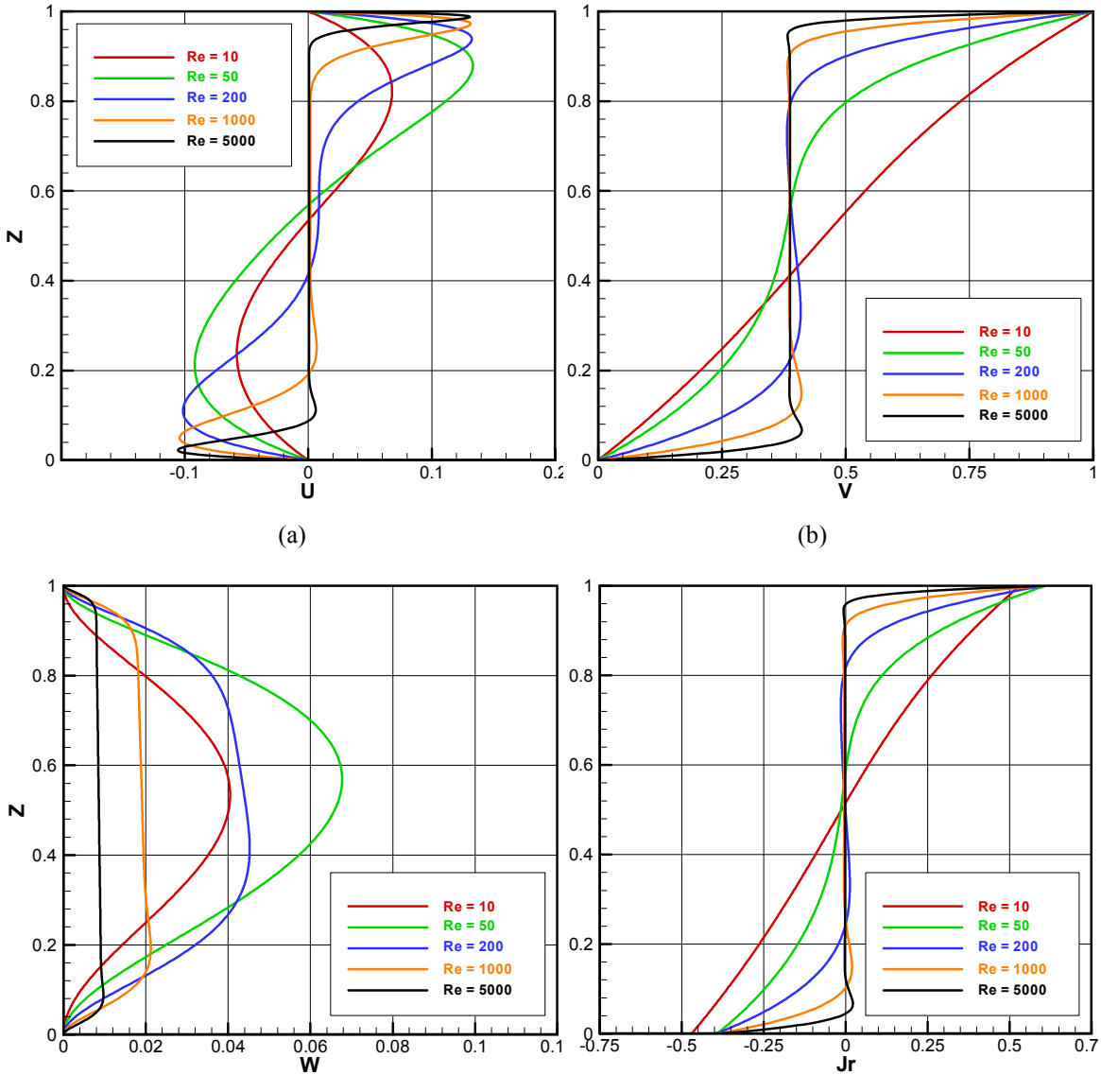

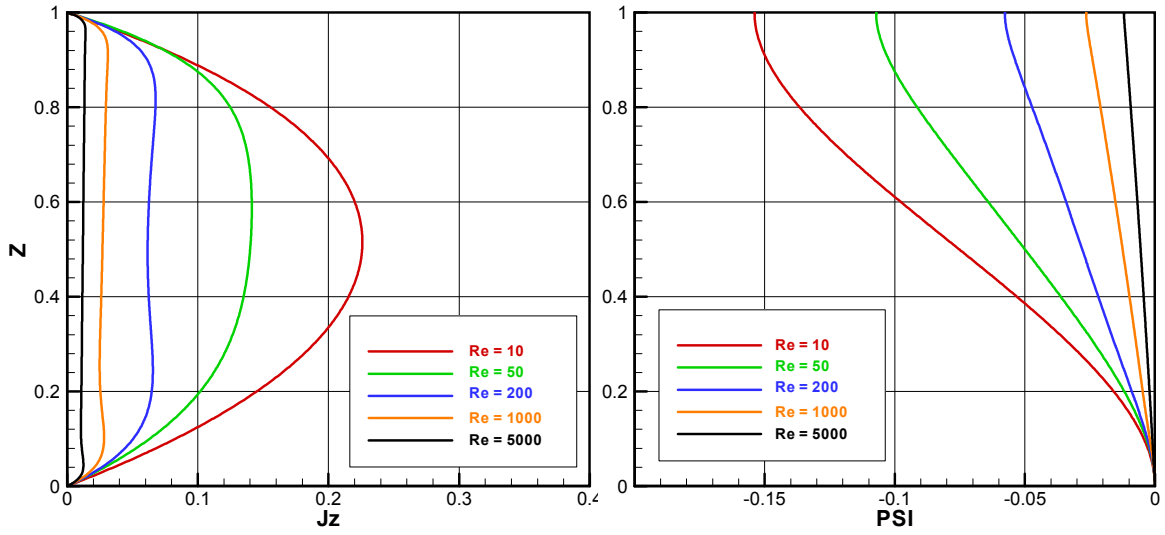

(e) (f)

Figure 7. *The profiles for the various Reynolds numbers at N = 0.3. (a) Radial component of velocity, (b) Azimuthal component of velocity, (c) Axial component of velocity, (d) Radial component of electric current density，(e) Axial component of electric current density，(f) Electric potential.*

Figure 8 shows the influence of the Hartmann number on the flow at *Re* = 5000. As increase in the Hartmann number, the azimuthal velocity at the core approaches the value of 0.5, while the radial velocity within the boundary layers is damped as increase in the Hartmann number. At a glance, the radial velocity in the core region seems to be zero as shown in (a), but its magnified figure indicates that the core velocity exhibits complicated behavior taking positive or negative values depending on the Hartmann number. This means that the core velocity is not a rigid-body-rotation flow but a slight spiral flow.

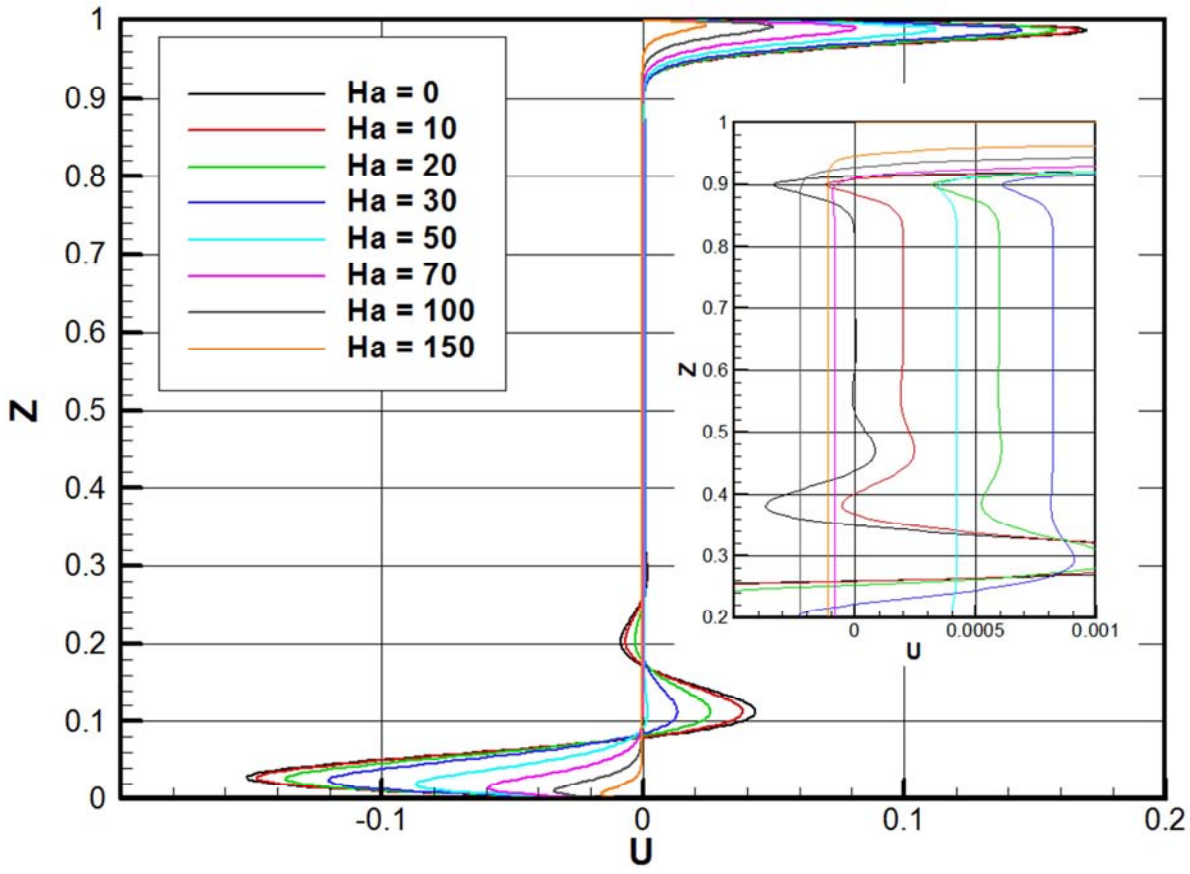

(a)

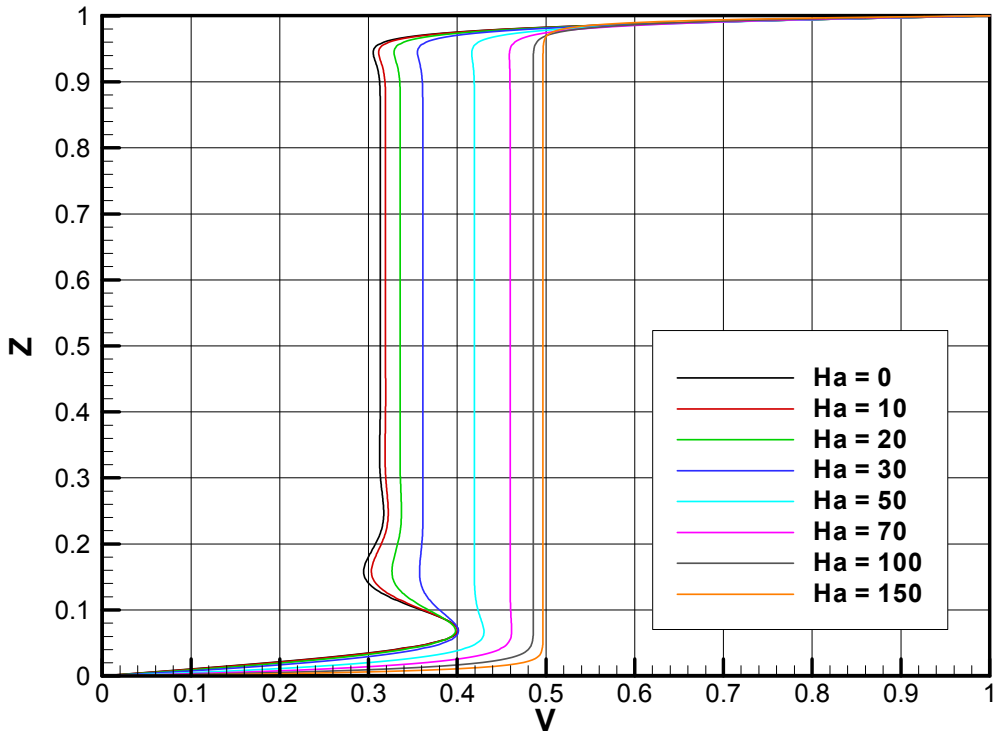

(b)

Figure 8. *Velocity profiles for the various Hartmann numbers at Re = 5000 for various Hartmann numbers. (a) Radial component of velocity, (b) Azimuthal component of velocity.*

5.4. Influence of the Conducting Disks on the Flow

Figures 9 and 10 show the influence of the conductance of the two disks on the three components of the velocity and axial electric current density at Re = 1000 and Ha = 10. For both cases, each figure shows the radial, azimuthal and axial components of velocity and axial component of electric current density. Although the Hartmann number is not very large, the velocity profiles vary significantly depending on the conductance of the disks. The azimuthal core velocity is about 0.34 for $C_K = 0$, but it increases as increase in the value of C_K. This is due to the suction of axial electric current density from the upper rotating disk. On the other hand, the effect of conductance of stationary disk, the azimuthal core velocity decreases as increase in the value of C_B. The reason for the effect of wall conductance ratios on the significant change in the azimuthal velocity could be qualitatively explained by considering Eqs. (42) and (49). In this study, using Eqs. from (34) to (49), any combinations between C_K and C_B are possible for obtaining the numerical results.

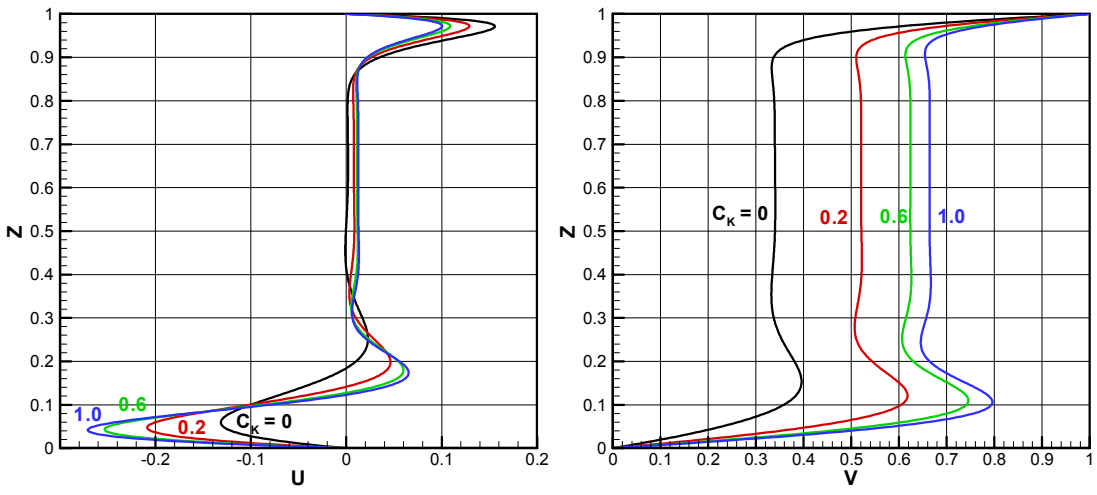

(a) (b)

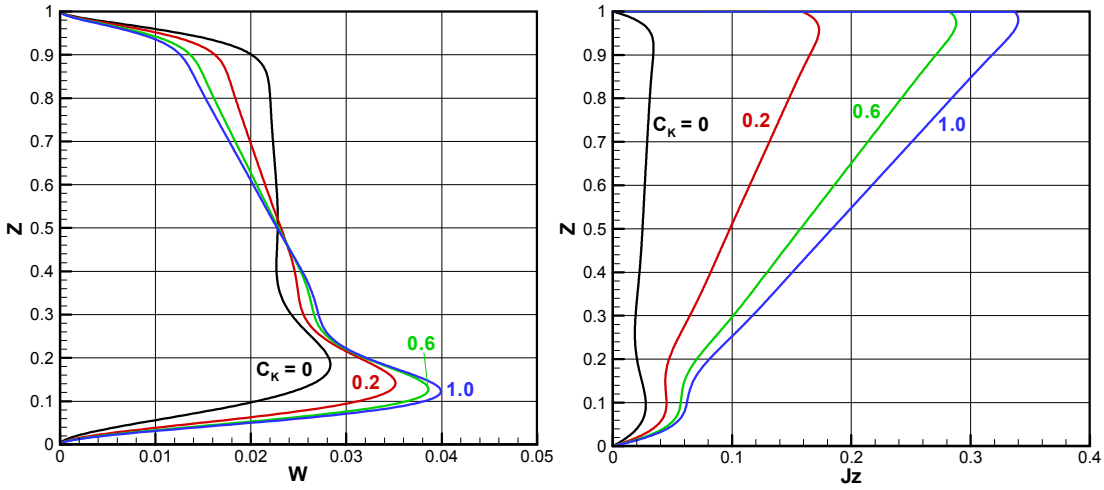

Figure 9. *Effect of the wall conductance ratios on the three components of velocity profile and axial electric current density at Re = 1000, Ha = 10 and $C_B = 0$ for various values of C_K. (a) Radial component of velocity, (b) Azimuthal component of velocity, (c) Axial component of velocity, (d) Axial component of electric current density.*

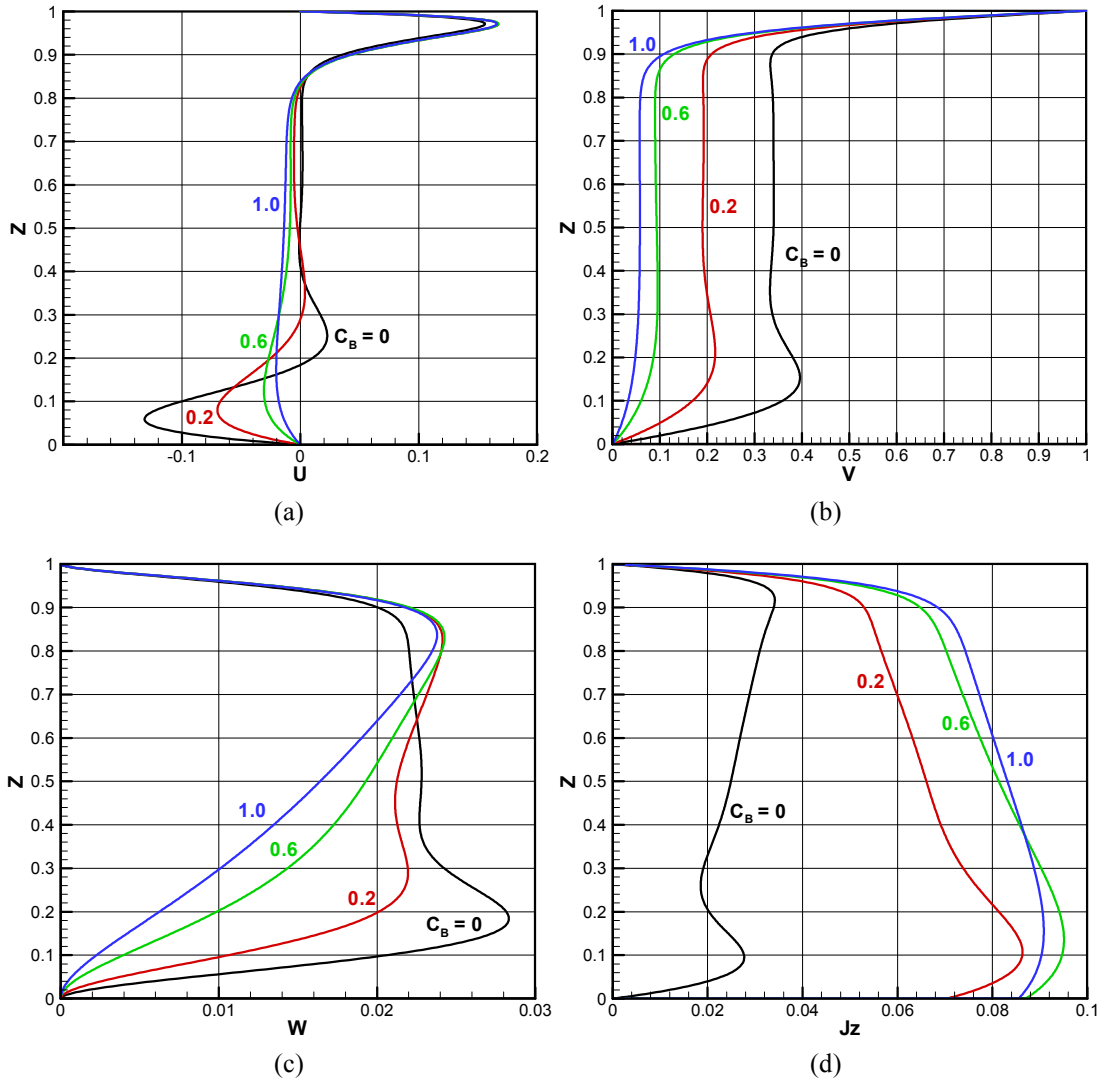

Figure 10. *Effect of the wall conductance ratios on the three components of velocity profile and axial electric current density at Re = 1000, Ha = 10 and $C_K = 0$ for various values of C_B. (a) Radial component of velocity, (b) Azimuthal component of velocity, (c) Axial component of velocity, (d) Axial component of electric current density.*

6. Conclusions

The magnetohydrodynamic flows in the gap between the coaxial rotating and stationary disks in the presence of a uniform axial magnetic field have been solved with the assumption of the Kármán's similarity and the followings results have been obtained.

1. The radial pressure gradient and the radial potential gradient, which do not vary along axial direction, must be obtained numerically so as to satisfy the continuity of mass and electric charge respectively.
2. In the limit of high Reynolds number cases, the fluid region can be divided into the distinct two boundary layers and a core region. The radial velocity in the core region is zero and the azimuthal one is about 0.313 when the magnetic effect is negligibly small.
3. When the interaction parameter N is much larger than unity and the disks are electrically insulated, the secondary flow is almost damped out and the azimuthal velocity in the core is nearly equal to 0.5.
4. Even for the high Reynolds number cases, the flow around $N = 1$ exhibits that the radial core velocity deviates from zero depending on the cases. This means that core velocity is not a rigid-body-rotation flow but a slight spiral flow.
5. The boundary condition for the electric current density penetrating the interface given in Eq. (42) allows us to obtain similarity solutions for various combinations of each wall conductance ratio. The influence of the wall conductance on the flow is quite significant.

Nomenclature

$\vec{B}$: Magnetic flux density vector [T]
b_0: Imposed magnetic flux density [T]
C: Wall conductance ratio [-]
d: Distance between the coaxial disks [m]
$\vec{e}_R$: Radial unit vector [-]
$\vec{e}_\theta$: Azimuthal unit vector [-]
$\vec{e}_Z$: Axial unit vector [-]
$\vec{f}$: Electromagnetic force vector [N/m^3]
f_R: Radial electromagnetic force [N/m^3]
f_θ: Azimuthal electromagnetic force [N/m^3]
f_Z: Axial electromagnetic force [N/m^3]
Ha: Hartmann number $=\sqrt{\sigma/\mu}\, b_0 d$ [-]
$\vec{j}$: Electric current density vector [A/m^2]
j_R: Radial current density [A/m^2]
j_θ: Azimuthal current density [A/m^2]
j_Z: Axial current density [A/m^2]
k_p: Constant for radial pressure gradient [Pa/m^2]
k_ψ: Constant for radial potential gradient [V/m^2]
N: Interaction parameter $= Ha^2/Re$ [-]
p: Pressure [Pa]
P: Dimensionless pressure [-]
r: Radial coordinate [m]
Re: Reynolds number $=\omega d^2/\nu$ [-]
t: Thickness of disk [m]
u: Radial component of velocity [m/s]
U: Dimensionless radial velocity $= u/(\omega r)$ [-]
v: Azimuthal component of velocity [m/s]
V: Dimensionless azimuthal velocity $= v/(\omega r)$ [-]
w: Axial component of velocity [m/s]
W: Dimensionless axial velocity $= w/(\omega r)$ [-]
z: Axial coordinate [m]
Z: Dimensionless axial coordinate $= z/d$ [-]
μ: Viscosity [Pa·s]
μ_m: Magnetic permeability [H/m]
ν: Kinematic viscosity = μ/ρ [m^2/s]
θ: Azimuthal angle [rad]
σ: Electric conductivity of fluid [1/(Ω·m)]
ρ: Density of fluid [kg/m^3]
ω: Angular velocity of rotating disk [rad/s]
Ω: Angular velocity of fluid rotation [rad/s]
ψ: Electric potential [V]
Ψ: Dimensionless electric potential [-]

Subscripts:

B: Bödewadt layer
c: Core region
K: Kármán layer
R: Partial derivative in radial direction

Appendix A

These ordinary equations shown below include the Coriolis force and Lorentz force. N indicates the interaction parameter and γ indicates the ratio between angular velocity of fluid and that of disk. If we set this value into zero, Karaman layer, which is formed in the vicinity of a rotating disk can be treated, while if we set it to minus one (-1), Bödewadt layer, which is formed near the stationary disk, is treated.

$$2U + \frac{dW}{d\eta} = 0$$

$$U^2 - V^2 + W\frac{dU}{d\eta} = \frac{d^2U}{d\eta^2} - NU + 2\gamma V$$

$$2UV + W\frac{dV}{d\eta} = \frac{d^2V}{d\eta^2} - NV - 2\gamma U$$

$$W\frac{dW}{d\eta} = -\frac{dP}{d\eta} + \frac{d^2W}{d\eta^2}$$

Boundary conditions:

$$\begin{cases} \eta \to \infty: \quad U = V = 0 \\ \eta = 0: \quad U = W = 0, \quad V = 1 \end{cases}$$

Dimensionless variables and non-dimensional numbers are defined as follows:

$$U(\eta) = \frac{u(r,z)}{\omega r}, \quad V(\eta) = \frac{v(r,z)}{\omega r}, \quad W(\eta) = \frac{w(z)}{\sqrt{\omega \nu}},$$

$$P(\eta) = \frac{p_2(z)}{\rho \omega \nu}, \quad \eta = z\sqrt{\frac{\omega}{\nu}}, \quad \gamma = \frac{\Omega}{\omega}, \quad N = \frac{\sigma b_0^2}{\rho \omega}$$

The numerical results for several values of interaction parameters are shown in Figure A1. Tables A1 and A2 show the numerical values for the Kármán flow and the Bödewadt flow respectively.

Table A1. *Numerical values obtained for the Kármán flow.*

η	U	V	W	P
0.000000	0.000000	1.000000	0.000000	0.000000
1.000000	0.180149	0.476618	-0.265529	-0.395470
2.000000	0.118843	0.203342	-0.573246	-0.401997
3.000000	0.058115	0.084519	-0.745273	-0.393959
4.000000	0.025665	0.034942	-0.825077	-0.391714
5.000000	0.010892	0.014432	-0.859617	-0.391258
6.000000	0.004548	0.005959	-0.874157	-0.391174
7.000000	0.001887	0.002461	-0.880209	-0.391158
8.000000	0.000781	0.001016	-0.882716	-0.391155
9.000000	0.000323	0.000420	-0.883753	-0.391155
10.000000	0.000133	0.000173	-0.884181	-0.391155
15.000000	0.000002	0.000002	-0.884479	-0.391155

Table A2. *Numerical values obtained for the Bödewadt flow.*

η	U	V	W	P
0.000000	0.000000	1.000000	0.000000	0.000000
1.000000	-0.478802	0.264581	0.624248	0.762501
2.000000	-0.328801	-0.192396	1.493165	-0.457221
3.000000	-0.036109	-0.271473	1.850009	-1.638988
4.000000	0.122681	-0.141337	1.732849	-1.746675
5.000000	0.121030	-0.001644	1.468749	-1.320643
6.000000	0.049953	0.057316	1.294546	-0.937838
7.000000	-0.008376	0.046999	1.259049	-0.775868
8.000000	-0.026777	0.014308	1.300525	-0.792140
9.000000	-0.017882	-0.007786	1.347812	-0.872536
10.000000	-0.003288	-0.012127	1.368512	-0.929834
20.000000	0.000102	0.000107	1.349498	-0.910776
30.000000	-0.000002	-0.000001	1.349598	-0.910705

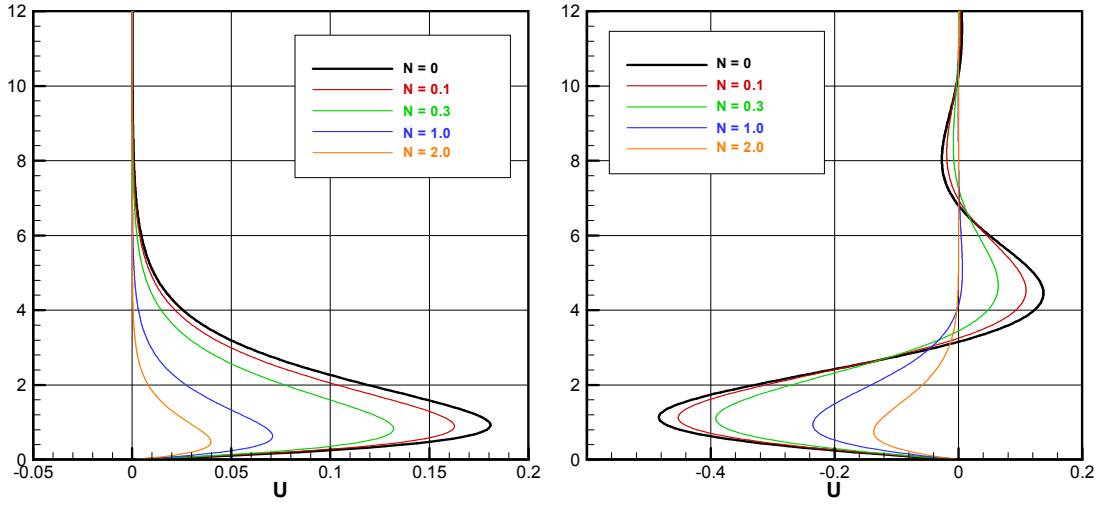

(a)

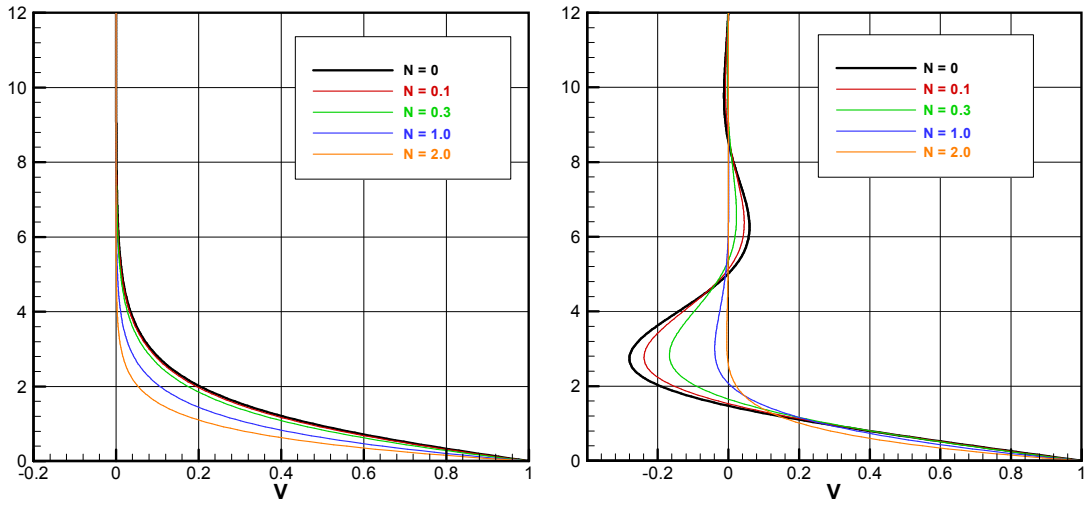

(b)

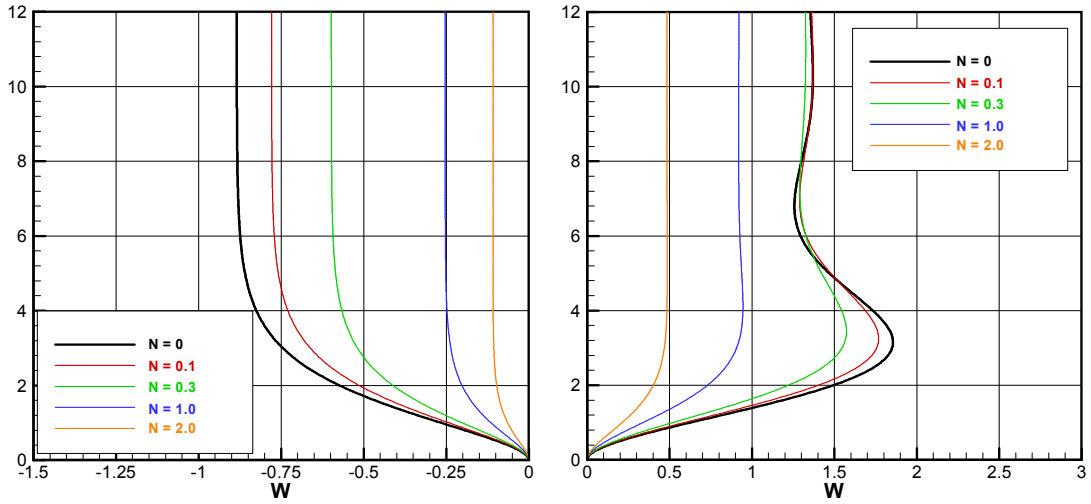

(c)

Figure A1. *Effect of the interaction parameter for the two types of the single-disk flow. The left-hand side indicates Kármán flow (γ = 0) and the right-hand-side Bödewadt flow (γ = -1). (a) Radial component of velocity, (b) Azimuthal component of velocity, (c) Axial component of velocity.*

References

[1] Th. von Kármán, "Über laminare und turbulente Reibung," ZAMM - Journal of Applied Mathematics and Mechanics/Zeitschrift für Angewandte Mathematik und Mechanik 1.4 (1921): pp. 233-252.

[2] W. G. Cochran, "The flow due to a rotating disc, "Mathematical Proceedings of the Cambridge Philosophical Society. Vol. 30. No. 03. Cambridge University Press, p. 1934.

[3] U. T. Bödewadt, "Die drehströmung über festem grunde," ZAMM - Journal of Applied Mathematics and Mechanics/Zeitschrift für Angewandte Mathematik und Mechanik 20.5 (1940): pp. 241-253.

[4] G. K. Batchelor, "Note on a class of solutions of the Navier-Stokes equations representing steady rotationally-symmetric flow," The Quarterly Journal of Mechanics and Applied Mathematics 4.1 (1951): pp. 29-41.

[5] K. Stewartson, "On the flow between two rotating coaxial disks," Mathematical Proceedings of the Cambridge Philosophical Society. Vol. 49. No. 02. Cambridge University Press, 1953.

[6] G. N. Lance and M. H. Rogers, "The Axially Symmetric Flow of a Viscous Fluid Between two Infinite Rotating Disk," Proceedings of the Royal Society of London A: Mathematical, Physical and Engineering Sciences. Vol. 266. No. 1324. The Royal Society, 1962.

[7] Carl E. Pearson, "Numerical solutions for the time-dependent viscous flow between two rotating coaxial disks," Journal of Fluid Mechanics 21.04 (1965): pp. 623-633.

[8] G. L. Mellor, P. J. Chapple and V. K. Stokes, "On the flow between a rotating and a stationary disk," Journal of Fluid Mechanics 31.01 (1968): pp. 95-112.

[9] Donald. Greenspan, "Numerical studies of flow between rotating coaxial disks," IMA Journal of Applied Mathematics 9.3 (1972): pp. 370-377.

[10] Lynn O. Wilson and N. L. Schryer, "Flow between a stationary and a rotating disk with suction," Journal of Fluid Mechanics 85.03 (1978): pp. 479-496.

[11] D. Dijkstra and G. J. F. Van Heijst, "The flow between two finite rotating disks enclosed by a cylinder," Journal of Fluid Mechanics 128 (1983): pp. 123-154.

[12] John F. Brady and Louis Durlofsky, "On rotating disk flow," Journal of fluid mechanics 175 (1987): pp. 363-394.

[13] G., P. Gauthier Gondret and M. Rabaud, "Axisymmetric propagating vortices in the flow between a stationary and a rotating disk enclosed by a cylinder," Journal of Fluid Mechanics 386 (1999): pp. 105-126.

[14] P. A. Davidson and A. Pothérat, "A note on Bödewadt–Hartmann layers," European Journal of Mechanics-B/Fluids 21.5 (2002): pp. 545-559.

[15] P. Moresco and T. Alboussière, "Stability of Bödewadt–Hartmann layers," European Journal of Mechanics-B/Fluids 23.6 (2004): pp. 851-859.

[16] C. J. Stephenson, "Magnetohydrodynamic flow between rotating coaxial disks," Journal of Fluid Mechanics 38.02 (1969): pp. 335-352.

[17] S. Kamiyama and A. Sato, "Magnetohydrodynamic FIow between Parallel Rotating Disks: Report 1, Influence of Finite Wall-Conductance," Bulletin of JSME 15.86 (1972): pp. 941-948.

[18] R. S. Agarwal and Rama Bhargava, "A numerical study of magnetohydrodynamic flow between a rotating and a stationary porous coaxial discs," Proceedings of the Indian Academy of Sciences-Section A. Part 3, Mathematical Sciences 88.5 (1979): pp. 399-407.

[19] S. Kishore Kumar, William I. Thacker and Layne T. Watson, "Magnetohydrodynamic flow between a solid rotating disk and a porous stationary disk," Applied Mathematical Modelling 13.8 (1989): pp. 494-500.